

Specific and Nonspecific Interactions in Ultraweak Protein–Protein Associations Revealed by Solvent Paramagnetic Relaxation Enhancements

Helle Johansson,[†] Malene Ringkjøbing Jensen,[‡] Henrik Gesmar,[§] Sebastian Meier,[¶] Joachim M. Vinther,^{†,⊥} Camille Keeler,[#] Michael E. Hodsdon,[#] and Jens J. Led^{*,†}

[†]Department of Chemistry, University of Copenhagen, Universitetsparken 5, DK-2100 Copenhagen Ø, Denmark

[‡]Univ. Grenoble Alpes, and CNRS, CEA, IBS, F-38044 Grenoble, France

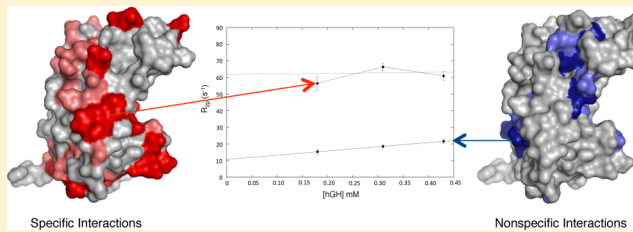
[§]Institute for Cellular and Molecular Medicine, University of Copenhagen, Blegdamsvej 3, DK-2200 Copenhagen N, Denmark

[¶]Carlsberg Laboratory, Gamle Carlsberg Vej 10, DK-1799 Copenhagen V, Denmark

[#]Department of Laboratory Medicine, Yale University School of Medicine, P.O. Box 208035, 333 Cedar Street, New Haven, Connecticut 06520-8035, United States

Supporting Information

ABSTRACT: Weak and transient protein–protein interactions underlie numerous biological processes. However, the location of the interaction sites of the specific complexes and the effect of transient, nonspecific protein–protein interactions often remain elusive. We have investigated the weak self-association of human growth hormone (hGH, $K_D = 0.90 \pm 0.03$ mM) at neutral pH by the paramagnetic relaxation enhancement (PRE) of the amide protons induced by the soluble paramagnetic relaxation agent, gadodiamide (Gd-DTPA-BMA). Primarily, it was found that the PREs are in agreement with the general Hwang-Freed model for relaxation by translational diffusion (*J. Chem. Phys.* 1975, 63, 4017–4025), only if crowding effects on the diffusion in the protein solution are taken into account. Second, by measuring the PREs of the amide protons at increasing hGH concentrations and a constant concentration of the relaxation agent, it is shown that a distinction can be made between residues that are affected only by transient, nonspecific protein–protein interactions and residues that are involved in specific protein–protein associations. Thus, the PREs of the former residues increase linearly with the hGH concentration in the entire concentration range because of a reduction of the diffusion caused by the transient, nonspecific protein–protein interactions, while the PREs of the latter residues increase only at the lower hGH concentrations but decrease at the higher concentrations because of specific protein–protein associations that impede the access of gadodiamide to the residues of the interaction surface. Finally, it is found that the ultraweak aggregation of hGH involves several interaction sites that are located in patches covering a large part of the protein surface.



INTRODUCTION

Protein–protein interactions are fundamental to most cellular processes. However, the interactions are often of surprisingly low affinity (K_D values in the mM to μM range), rendering detailed studies extremely difficult using conventional biophysical techniques. Examples of low-affinity complexes are the transient complexes between proteins involved in electron transfer,^{1–3} enzyme–substrate complexes,^{4,5} and weak protein self-associates.^{6–9}

In recent years our insight into the formation and dynamics of weak protein–protein interactions has increased considerably owing to a series of pioneering studies using paramagnetic NMR relaxation enhancement (PRE).^{1,2,4,5,9–15} These studies contrast cosolute paramagnetic NMR studies of the formation of more stable protein complexes^{16,17} (K_D in the nM range) by providing detailed information about the

interaction process. Thus, they showed that weak protein–protein associations, including both interactions between nonidentical and identical proteins (protein self-association), can be viewed as a two-step process comprising the initial formation of an ensemble of transient, nonspecific encounter complexes dominated by electrostatic forces, followed by a rearrangement along the protein surface, to form a final, well-defined complex stabilized by short-range hydrophobic interactions and hydrogen bonds in addition to the electrostatic forces.^{18–20} Mechanistic details of a protein–protein association pathway were also obtained by PRE titration measurements.⁵

Received: September 20, 2013

Published: June 27, 2014

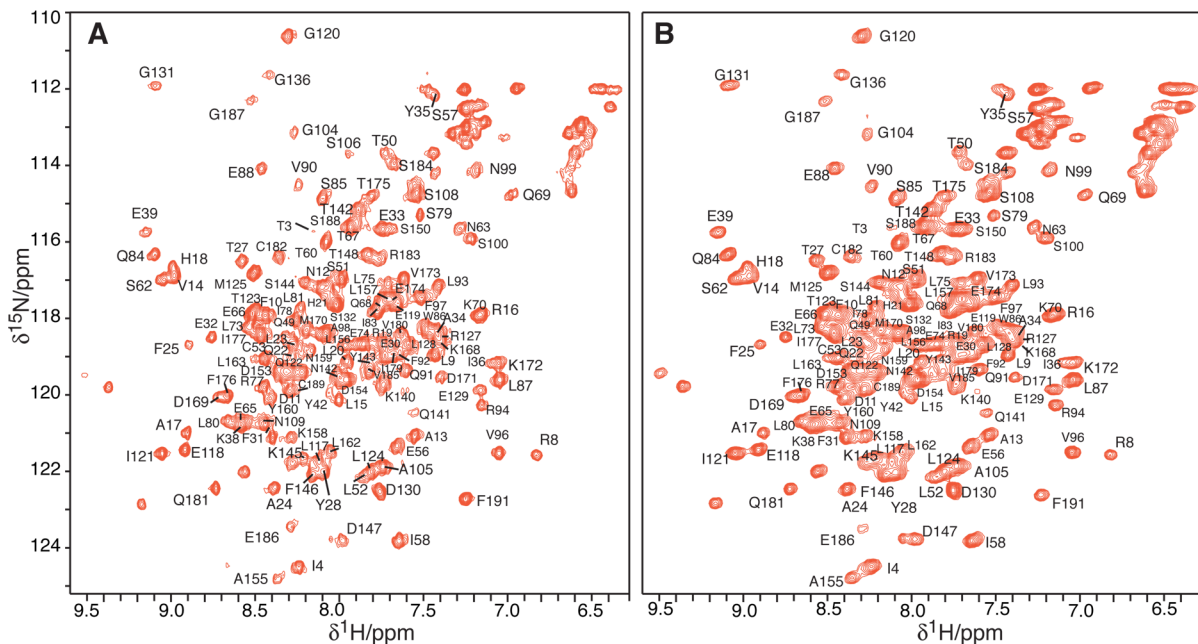


Figure 1. ^1H - ^{15}N HSQC spectra of hGH at 25 °C and pH 7.0: (A) 0.126 mM hGH without gadodiamide; (B) 0.430 mM hGH in the presence of 4.0 mM gadodiamide.

Here we use the self-associating human growth hormone (hGH) as a model system for weak protein–protein interactions. Previously,⁸ an investigation of the hGH self-association using ^{15}N NMR relaxation showed that only ultraweak oligomers were formed under the applied experimental conditions (0.11–0.58 mM hGH, pH 7, 40 mM salt), including a dimer with $K_D = 0.90 \pm 0.03$ mM, and a small fraction of trimers or tetramers. In agreement with these ultraweak complex formations only small chemical shift changes ($\Delta\delta_{1\text{H}} < 0.02$ ppm and $\Delta\delta_{1\text{SN}} < 0.2$ ppm) were observed in the applied concentration range, primarily at the two ends of the hGH molecule.⁸

To investigate the self-association of hGH we monitored the protein–protein interaction as a function of the protein concentration by measuring the highly sensitive, transverse PRE (R_{2p}) of the backbone NH protons at increasing hGH concentrations and a constant concentration of the soluble, overall uncharged paramagnetic Gd^{3+} relaxation agent gadodiamide (Gd(DTPA-BMA)).²¹ This approach differs from previous PRE studies of weak protein–protein interactions where paramagnetic spin labels were bound covalently to one of the two interacting proteins,^{1,2,4,5} and from the studies of more stable complexes where the protein concentration was kept constant while varying the concentration of the cosolute paramagnetic relaxation agent.^{16,17} The approach here is attractive for several reasons. First, it is experimentally simple since no paramagnetic spin labeling or chemical modification of the protein is required. Second, it excludes risks of imposing structural disturbances. Third, as demonstrated below, the use of a constant concentration of the soluble relaxation agent combined with a varying protein concentration allows a distinction between surface residues that are involved in the formation of weak specific complexes and residues that are affected only by nonspecific electrostatic interactions. This conclusion requires a clarification of the theoretical model that describes the experimental PREs. To that end, we have first examined the applicability of the general

Hwang-Freed model for spin relaxation by translational diffusion^{22,23} to describe the PREs of the protein system investigated here.

THEORY

The PREs caused by cosolute paramagnetic relaxation agents are controlled by the molecular translational diffusion and the electron relaxation rate. Luz and Meiboom first addressed the case of diffusional relaxation controlled by the electron relaxation rate.²⁴ They found that the solvent PREs can be evaluated by simply integrating the Solomon equations for the electron nucleus dipole–dipole relaxation²⁵ from the distance of closest approach, d , between the electron and the nucleus to infinity. Later, Hwang and Freed proposed a general model for spin relaxation by translational diffusion in liquids, in which pair-correlation functions, related to a potential of averaged forces between the molecules, are considered.^{22,23,26}

Here, the Hwang-Freed model was used to analyze the experimental paramagnetic relaxation data of hGH. According to this model the R_{2p} rates (the transverse PREs) are given by²⁶

$$R_{2p} = \frac{16}{405} \pi \left(\frac{\mu_0}{4\pi} \right)^2 \frac{1000 N_A [M] \tau_D \gamma_1^2 g_e^2 \mu_B^2 S(S+1)}{d^3} \times \{4J(0) + 13J(\omega_S) + 3J(\omega_1)\} \quad (1)$$

where μ_0 is the magnetic permeability of free space, N_A is the Avogadro constant, $[M]$ is the concentration of the paramagnetic relaxation agent, τ_D is the diffusional correlation time for the interaction between electrons of the relaxation agent and the backbone amide protons of hGH, γ_1 is the nuclear gyromagnetic ratio, g_e is the g -value of the electron, μ_B is the Bohr magneton, S is the spin quantum number of the unpaired electrons, d is the distance of closest approach between the paramagnetic center and the observed nucleus, ω_1 is the nuclear Larmor frequency, and ω_S is the electron Larmor frequency. The general expression for the spectral density function, $J(\omega)$, is given by^{23,26,27}

$$J(\omega) = \text{Re} \left\{ \frac{1 + s/4}{1 + s + 4s^2/9 + s^3/9} \right\} \quad (2)$$

where

$$s = \{\tau_D(i\omega + 1/\tau_s)\}^{1/2} \quad (3)$$

τ_s being the electron relaxation time. Below we demonstrate that the Hwang-Freed model describes the experimental R_{2p} rates for the amide protons of hGH, when the dependence of τ_D on molecular crowding effects^{28–30} in the viscous protein solution is taken into account.

■ RESULTS AND DISCUSSION

Measurement of Experimental Solvent PREs in hGH. The previous assignment of the backbone amide ^{15}N signals³¹ was extended using a TCI cryoprobe-equipped 800 MHz spectrometer with an approximately four times higher sensitivity than the 500 MHz spectrometer used previously.⁸ This results in an improved resolution and increased sensitivity. Thus, using the 800 MHz spectrometer and a hGH concentration of 0.175 mM the sequential assignment was extended from 60% to 78% of the nonproline backbone amide ^{15}N signals. Figure 1A shows the assignments of the $^1\text{H}-^{15}\text{N}$ HSQC spectrum of a 0.126 mM hGH sample. The assigned chemical shifts are given in Supporting Information Table S1.

A gadodiamide concentration was determined that is sufficiently large to allow accurate measurements of the ^1H R_{2p} rates of hGH without jeopardizing the spectral resolution. From a series of ^{15}N HSQC spectra of a 0.430 mM hGH sample at pH 7.0, 298 K and a gadodiamide concentration between 0 mM and 11.0 mM, a gadodiamide concentration of 4.0 mM was chosen as the best compromise (Figure 1B).

The R_2 relaxation rates of the backbone amide protons of 127 hGH residues in the presence of 4.0 mM paramagnetic gadodiamide ($R_{2\text{exp}}$) were measured at the three hGH concentrations, 0.180 mM, 0.310 mM, and 0.430 mM (Supporting Information Table S2). The remaining 64 residues were either not assigned (including 8 prolines) or the R_2 rates of the amide protons could not be determined. The rates in the absence of gadodiamide (R_{2d}) were measured at 0.126 mM and 0.460 mM hGH (Supporting Information Table S3). Since the R_{2d} rates vary linearly with the hGH concentration in the applied concentration range,⁸ the R_{2d} rates at 0.180 mM, 0.310 mM, and 0.430 mM were obtained from the values at 0.126 mM and 0.460 mM hGH by linear interpolation. The R_{2p} rates (Supporting Information Table S4) derived from the experimental rates (eq 7, Materials and Methods) vary from 7 s^{-1} to 91 s^{-1} .

Describing the Gadodiamide-Induced R_{2p} Rates of hGH by the Hwang-Freed Model. To describe the gadodiamide-induced R_{2p} rates (PREs) of hGH using the Hwang-Freed model, we must evaluate the impact of the crowding effects on the diffusion of hGH and gadodiamide. In the Hwang-Freed model,^{22,23} the correlation time for relaxation by translational diffusion, τ_D is given by

$$\tau_D = \frac{d^2}{D_G + D_p} \quad (4)$$

where D_G and D_p are the translational diffusion coefficients of gadodiamide and hGH, respectively, given by

$$D_G = kT/(6\pi a_G \eta) \quad D_p = kT/(6\pi a_p \eta) \quad (5)$$

and T is the temperature, k is the Boltzmann constant, a_G and a_p are the hydrodynamic radius of gadodiamide and hGH, respectively, and η is the translational viscosity. If the diffusion of gadodiamide is unaffected by the protein, $D_G \gg D_p$ because of the smaller size of the gadodiamide molecule and D_G will control τ_D . However, with increasing protein concentration the diffusion of both the small cosolute and the protein are reduced several-fold compared to their diffusion in water, because of crowding effects caused by transient association of the cosolute to the less mobile protein molecules, by weak associations between the protein molecules, and by molecular collisions.^{28–30,32} Specifically, a recent study of the protein binding of gadolinium contrast agents suggested that gadodiamide, and Gd-based relaxation agents in general, associate weakly to proteins.³³ These observations are supported by a study of gadodiamide induced PREs in ubiquitin²¹ that was based on an empirical grid search and the Solomon equations for dipolar relaxation modulated by rotational reorientation.²⁵ It was suggested that the PREs of the protein nuclei can be described as a second sphere interaction, where gadodiamide forms a nonspecific, yet rotationally correlated, adduct with the protein in which the dipolar coupling between the electronic spin and the ^1H spin is modulated by the molecular rotation of the protein, the electron relaxation, and the lifetime of the adduct. These results suggest a reduced translational diffusion of gadodiamide near the protein. This reduction, as well as the reduction of the protein diffusion, must be taken into account (eq 4) when using the Hwang-Freed model to describe the relaxation of protein nuclei caused by a cosolute paramagnetic relaxation agent.

Theoretical PREs were estimated as a function of the distance of closest approach, d , at the three applied hGH concentrations and at infinite hGH dilution (monomeric hGH) using the Hwang-Freed model (eqs 1, 2, 3, 4, 5) and the fraction of monomers and dimers. It was assumed that the monomer–dimer exchange is fast on the time scale of the R_2 measurement. Therefore, the PREs are a weighted average of the PREs of the monomers and dimers, the weights being the fractions of hGH involved in each one of the two forms at the specific concentrations

$$R_{2p} = FM \times R_{2p,\text{monomer}} + FD \times R_{2p,\text{dimer}} \quad (6)$$

The fractions of hGH molecules present as monomers, FM, and as dimers, FD, were derived from the dimer dissociation constant $K_D = 0.90 \pm 0.03 \text{ mM}$,⁸ as detailed in Supporting Information and are 0.767 and 0.233 at $[\text{hGH}] = 0.180 \text{ mM}$, 0.677 and 0.323 at $[\text{hGH}] = 0.310 \text{ mM}$, and 0.626 and 0.374 at $[\text{hGH}] = 0.430 \text{ mM}$. It was assumed that only monomers and dimers are present. The fractions were used to calculate the R_{2p} rates (PREs) at 298 K and a ^1H frequency of 800 MHz for the applied gadodiamide concentration (4 mM) and the electron spin of gadolinium (7/2). The electron relaxation time of Gd^{3+} ($\tau_s = 1/R_{2s} = 3.7 \text{ ns}$)³⁴ was used as the correlation time for the electron-nucleus interaction.

Figure 2 shows the R_{2p} rates as a function of the distance of closest approach, d , for three cases of diffusion. In A (lower dashed curves), the translational diffusion coefficient of gadodiamide in pure water at 298 K ($D_G = 4.5 \times 10^{-10} \text{ m}^2/\text{s}$)³⁵ was used. In that case, D_G controls τ_D since $D_G \gg D_p$. Therefore, the R_{2p} rates are relatively small and independent of the hGH concentration. In B, it was assumed that $D_G = D_p$, corresponding to a correlated motion of gadodiamide and the protein. D_p was calculated from the hydrodynamic radius of

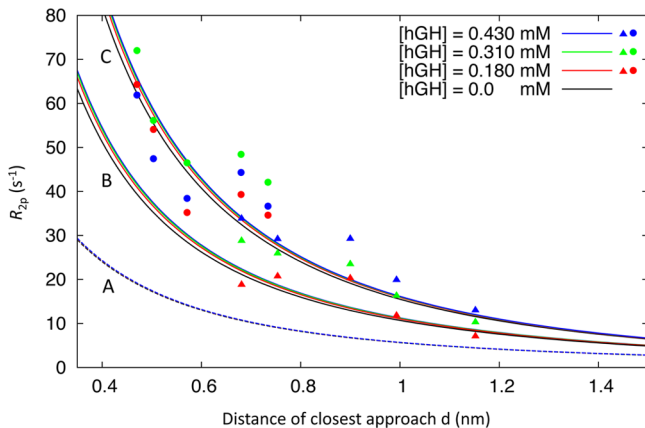


Figure 2. Theoretical R_{2p} rates versus distance of closest approach, d , for the three applied hGH concentrations and hGH at infinite dilution, and for three different cases of diffusion regimes, (A), (B), and (C), together with the experimental R_{2p} rates of ten selected hGH residues. The radius of gadodiamide, 0.35 nm, was used as the shortest d value. The theoretical R_{2p} rates were calculated using the Hwang–Freed model for relaxation by translational diffusion and the experimental conditions used in the study (see text). The three cases correspond to three different diffusion coefficients: (A) D_G in pure water; (B) $D_G = D_p$ corresponding to a rotationally correlated motion of gadodiamide and the protein; (C) the diffusion coefficients (D_p and D_G) were reduced by a factor of 2 compared to the diffusion of hGH in pure water, while retaining the condition $D_G = D_p$. Ten experimental R_{2p} rates versus d are indicated by bullets and triangles. The d values were calculated from the crystal structure of hGH (see text). Bullets are R_{2p} rates that decrease for $[hGH] > 0.310 \text{ mM}$ (see text). They correspond to residues that are relatively close to the surface and are from left to right A155, E39, S62, D154, and D130. The triangles are R_{2p} rates that increase in the entire concentration range (see text). They correspond to residues that are relatively far from the surface and are from left to right L15, R178, H21, M170, and L80.

hGH, a_{hGH} , and the viscosity of pure water at 298 K ($\eta_{\text{water}} = 9 \times 10^{-4} \text{ Pa s}$),³⁶ using eq 5, while a_{hGH} , in turn, was estimated from the Stokes–Einstein equation for the rotational motion of a spherical molecule,^{37,38} that is, $a_{hGH} = [(\tau_{R,hGH} \times 3kT)/(4\pi \times \eta_{\text{water}})]^{1/3}$. For the monomer, the correlation time at infinite hGH dilution, $\tau_{R,hGH} = 13.4 \text{ ns}$, was used. This value was obtained previously⁸ under the same experimental conditions as used here. Finally, D_p for the hGH dimer was estimated assuming that $\tau_{R,hGH}$ of the dimer is twice that of the monomer, that is, 26.8 ns. The calculated hydrodynamic radii of the hGH monomer and dimer were $2.4 \times 10^{-9} \text{ m}$ and $3.1 \times 10^{-9} \text{ m}$, respectively, while the corresponding diffusion coefficients were $D_{p,\text{mon}} = 9.8 \times 10^{-11} \text{ m}^2/\text{s}$ and $D_{p,\text{dim}} = 7.8 \times 10^{-11} \text{ m}^2/\text{s}$. In C, the full crowding effect was implemented. Thus, in addition to the condition $D_G = D_p$ the translational diffusion is reduced. Previously, Dauty and Verkman³² have found comparable reduction in the translational diffusions of small solutes and proteins. Therefore, both diffusion coefficients (D_p and D_G) were reduced arbitrarily by a factor of 2 compared to the diffusion of hGH in pure water, in accordance with previous results,^{30,32} while still retaining the condition $D_G = D_p$. This D_G value is the minimum translational diffusion coefficient for gadodiamide for a given value of D_p . In general, small cosolutes sense the viscosity of the local environment,^{29,32} e.g., near the protein surface, while the protein senses a general viscosity of the solution.³² Therefore, D_G might be larger than D_p .

Figure 2 also shows the experimental R_{2p} rates for ten hGH residues as a function of the distance of closest approach, d , that cover the experimental R_{2p} range. The distances from a given amide proton to the nearest point on the surface of hGH were obtained using the crystal structure of hGH (3HHR). Initially, conformations of the missing loop at residues 149–153 were built using the ArchPRED server³⁹ and protons were added to the crystal structure. Subsequently, the MSMS computer program⁴⁰ was used to calculate the solvent excluded surface of hGH using a probe size of 0.35 nm, and the distances from the amide protons to the surface were extracted using a script available under the Biopython distribution.⁴¹ Finally, d was calculated as the sum of the distance from the surface and the hydrodynamic radius of gadodiamide (0.35 nm). The d -values for all the amide protons are given in Supporting Information Table S7.

Several conclusions can be drawn from Figure 2. First, the theoretical curves show that the R_{2p} rates increase considerably with increasing crowding effect and, thereby, with increasing protein concentration. Second, the R_{2p} rates increase only slightly with increasing rotational correlation of the protein, as revealed by the small concentration dependence of the rates within the individual bundles of plots (case B and C). None of these concentration dependent increases are present, if τ_D is controlled entirely by the gadodiamide diffusion coefficient in pure water (case A). Third, the experimental R_{2p} rates cover the same range as the theoretical R_{2p} rates. Fourth, the experimental R_{2p} rates are all significantly larger than case A, that is, the crowding reduces the diffusion of gadodiamide and the protein considerably and thereby increases the R_{2p} rates. Finally, the amide protons with decreasing R_{2p} rates in the 0.310–0.430 mM concentration range (see below) correspond to residues that are relatively close to the surface (bullets), while those with constantly increasing R_{2p} rates (see below) correspond to residues that are relatively far from the surface (triangles). Altogether, Figure 2 clearly shows that the Hwang–Freed model describes the gadodiamide-induced R_{2p} rates in proteins, if the crowding effects are taken into account.

Monitoring Protein–Protein Interactions by Cossolute Paramagnetic Relaxation. Primarily, it was found that the experimental R_{2p} rates vary substantially among the residues, suggesting a large dispersion in the accessibility of gadodiamide. Second, for most of the residues the rates vary considerably within the applied concentration range, indicating significant interactions between the hGH molecules and/or between hGH and gadodiamide. The variations of the experimental R_{2p} rates with the hGH concentration follow two different patterns. Thus, the rates of about 60% of the observed residues *increase* in the entire concentrations range in agreement with an increasing crowding effect, while the rates of about 40% of the residues *increase* only in the 0.180–0.310 mM concentration range but *decrease* between 0.310–0.430 mM (Supporting Information Table S4), in agreement with a reduced accessibility for gadodiamide. The R_{2p} rates were classified as decreasing if the average slope is negative, or if the rate at 0.430 mM is smaller than the rate at 0.310 mM. Also, the latter rates are defined as decreasing if the experimental rate at 0.310 mM exceeds the average of the rates at 0.180 mM and 0.430 mM ($R_{2p}(\text{av})$) by more than two standard deviations, that is, $\Delta/\sigma_\Delta > 2$, where $\Delta = R_{2p}(0.310 \text{ mM}) - R_{2p}(\text{av})$. The estimated uncertainties are given by $\sigma_\Delta = [\sigma_{R_{2p}(0.310 \text{ mM})}^2 + \sigma_{R_{2p}(\text{av})}^2]^{1/2}$. A few adjacent residues within the same interaction surface, but

with slightly smaller Δ/σ_Δ ratios, were also included. The equations used to estimate the nonlinear concentration dependence of R_{2p} , $R_{2p}(\text{av})$, and $\sigma_{R_{2p}(\text{av})}$ are given in materials and methods, and the calculated Δ and σ_Δ values are given in Supporting Information Table S6.

To understand the experimental R_{2p} rates and their concentration dependence, it is useful to consider how the cosolute paramagnetic relaxation agent affects the relaxation of the protein nuclei. At a sufficiently low protein concentration, where the protein is monomeric, gadodiamide has free access to the entire surface of the protein and the R_{2p} rates will depend only on the distance of the amide protons from the surface of the monomer. With increasing protein concentration, long-range electrostatic interactions between the protein molecules lead to the formation of transient, nonspecific encounter complexes, and a two-dimensional search along the protein surfaces by the interacting hGH molecules.^{2,3,10,11,19,20,42,43} These transient interactions will increase the crowding near the protein surface, and by that reduce the rate of diffusion, including that of gadodiamide, and increase the R_{2p} rates of the hGH amide protons. However, the increasing protein concentration may also result in specific associations stabilized by short-range, hydrophobic interactions and hydrogen bonds, in addition to the ubiquitous long-range electrostatic interactions. In that case, the protein molecules will be kept in close proximity to one another for a prolonged period of time. This will reduce the accessibility of gadodiamide to the protein considerably and thereby decrease the R_{2p} rates of the protein nuclei.

Nonspecific Transient Interactions. The observed increases of the R_{2p} rates that result from a reduced diffusion caused by the crowding effects have different slopes (Figure 3, Supporting Information Table S5). This finding indicates that the crowding effects vary along the surface of the protein molecule. Since the small cosolute senses the local viscosity and the local crowding effect, while the protein senses the general viscosity of the solution,³² only D_G reflects the differences in the local crowding effects along the surface of the protein molecule. These differences are in agreement with the nonspecific, transient interactions between the hGH molecules, which also must vary with the locations because of their differences in electrostatic character and geometry along the surface, and will therefore lead to a variation in the local crowding effect close to the protein. Furthermore, the fact that all the R_{2p} rates increase in the lower hGH concentrations from 0.180 mM to 0.310 mM supports the nonspecific and transient nature of the interactions. Finally, it should be noted that the differences in the local crowding must be taken into account when the solvent PREs are used in structure calculations of protein–protein complexes. Previously, it was assumed that the solvent PREs are determined only by the diffusion of gadodiamide in pure water,¹⁷ corresponding to a considerably higher and uniform diffusion in pure water (case A, Figure 2).

Most of the residues with linearly increasing R_{2p} rates are located in regions where the hGH molecule is less accessible to other bulky protein molecules for short-range interactions, but where the local crowding effects still affect the diffusion of the gadodiamide and its long-range paramagnetic interaction with the residues. This holds in particular for the inaccessible inner residues in the four-helix core that stabilizes hGH through intramolecular hydrophobic interactions,⁴⁴ that is, A17, L20, A24, L76, S79, I83, W86, V90, L117, I121, L124, D169, M170,

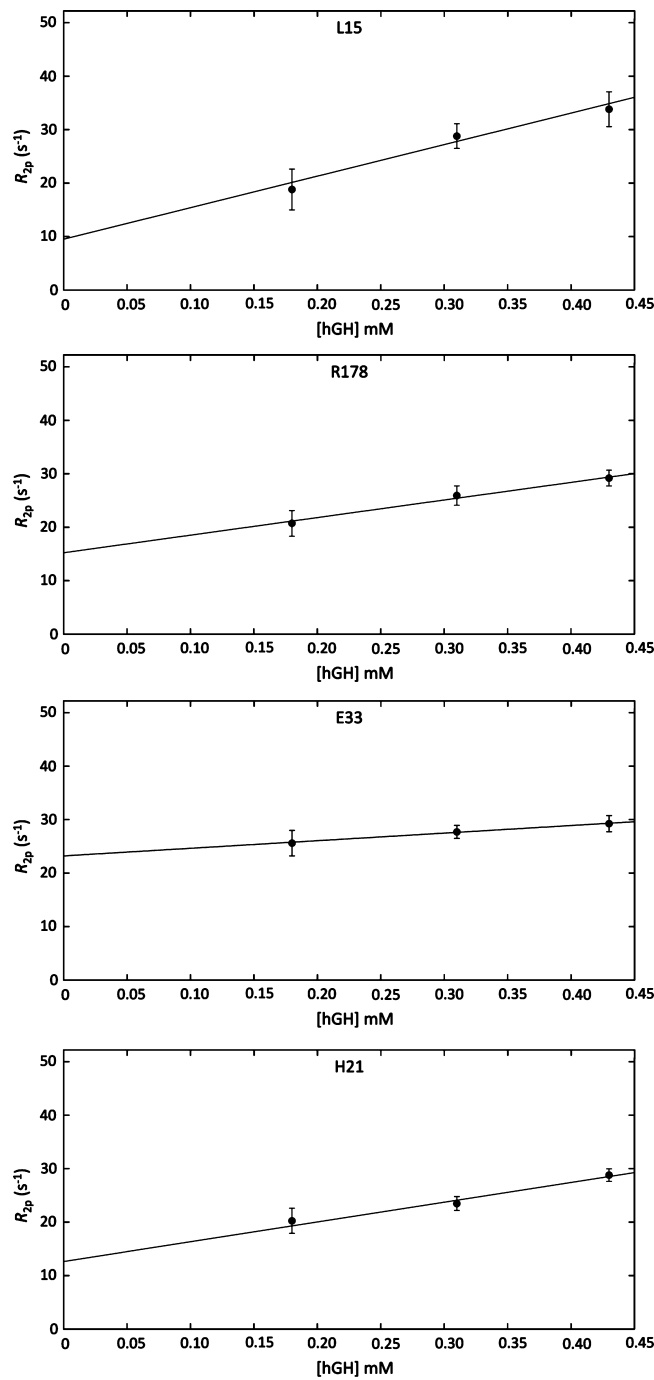


Figure 3. Examples of R_{2p} rates that increase linearly with the hGH concentration in the entire experimental concentration range. The straight solid lines are least-squares fit of the rates. The four residues are located in less accessible grooves on the surface of the hGH molecule (Figure 4). The slopes of the hGH dependencies of the four R_{2p} rates are (in $s^{-1} \times mM^{-1}$) L15, 59 ± 13 , R178, 33 ± 4 , E33, 14 ± 1 , H21, 37 ± 6 .

V173, L177, and V180 (Figure 4A and B), all of which have R_{2p} rates that increase linearly with the hGH concentration. Also, a large part of the surface residues have linearly increasing R_{2p} rates. These residues are located in major or minor surface grooves (Figure 4C and D), where the hGH molecule is less accessible. Some of these residues are charged at the neutral pH, which increases their tendency to participate in intermolecular electrostatic interactions. Thus, the two groups

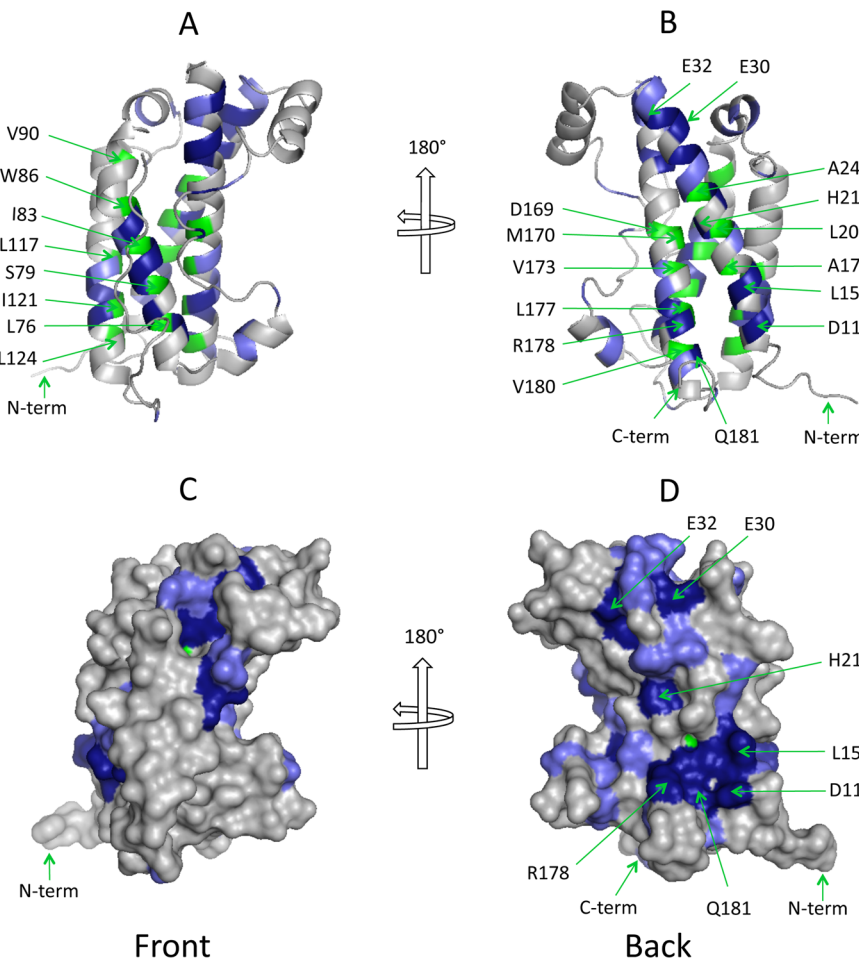


Figure 4. Residues with linearly increasing R_{2p} rates mapped onto the structure of hGH (pdb: 3HHR); A and B are ribbon models; C and D are surface representations. The less accessible surface residues ($R_{2p}(0) \leq 20 \text{ s}^{-1}$) are dark blue; the more accessible surface residues ($R_{2p}(0) > 20 \text{ s}^{-1}$) are slate blue; the low accessible core residues of the four-helix bundle are green. The ribbon models show the four major helices (helix 1, residues 9–34; helix 2, residues 72–92; helix 3, residues 106–128; and helix 4, residues 155–184), the three small helices (residues 38–47, 64–70, and 94–100), the two major loops (residues 45–63 and 128–148), and the minor loop (residues 100–105). Notice that the inner, stabilizing residues of the four-helix bundle are hidden in the surface representation.

of sequentially distant residues, D11, M14, L15 and R178, Q181, form a common patch with low accessibility in a groove on the concave surface at the lower end of the molecule. Similarly, E30, F31, E32, and E33 are all located in grooves at the top of the molecule, while H21 is located in a groove at the center.

Formation of Specific Complexes. The decreases of the R_{2p} rates of approximately 40% of the residues in the 0.310–0.420 mM hGH concentration range (Supporting Information Table S6) indicate the formation of specific and relatively stable protein–protein associates that might be stabilized by short-range, hydrophobic interactions and hydrogen bonds, as discussed above. Examples of R_{2p} rates that decrease in the 0.310–0.430 mM concentration range are shown in Figure 5. The formation of specific protein–protein associates is supported by two additional characteristics. First, all the residues with decreasing R_{2p} rates are located on or close to the surface of the protein (Figure 2, Supporting Information Table S7), and with rates that are significantly larger than the constantly increasing rates (Figures 2 and 3, and Supporting Information Table S4). Second, most of the residues are confined to the convex side of the molecule (Figure 6) and mainly to three large patches, one at each end of the molecule,

and one on the front or convex side of the molecule including residues from the two major loops (residues 45–63 and 128–148). Protein–protein interaction with the patches at the two ends is supported by small concentration dependent chemical shift changes observed previously.⁸ On the opposite, concave side only a few residues with decreasing R_{2p} rates are located, including R16, H18, and D171. These observations together suggest that the residues with the decreasing R_{2p} rates are part of weak binding interfaces of specific hGH-hGH complexes.

The patch at the bottom of the molecule (patch 1, Figure 6A) forms a large and flat interface as normally found for interfaces in oligomeric proteins.⁴⁵ Although the data do not reveal which interface residues are energetically most important for the interaction (the hot spot),⁴⁶ the positively charged residue R183 and the negatively charged residue D130 could play an important role by steering the interaction partner into position by long-range electrostatic forces. Subsequently, the adjacent uncharged, polar residues S184 and S132 and S71 and the adjacent, hydrophobic residue L73, all of which are found frequently in hot spots,⁴⁷ could stabilize the specific encounter complex through short-range hydrogen bonds and hydrophobic interactions. The spatially adjacent residues, I4, R8, E65, Q69, G126, R127, L128, and E129, which also have decreasing R_{2p}

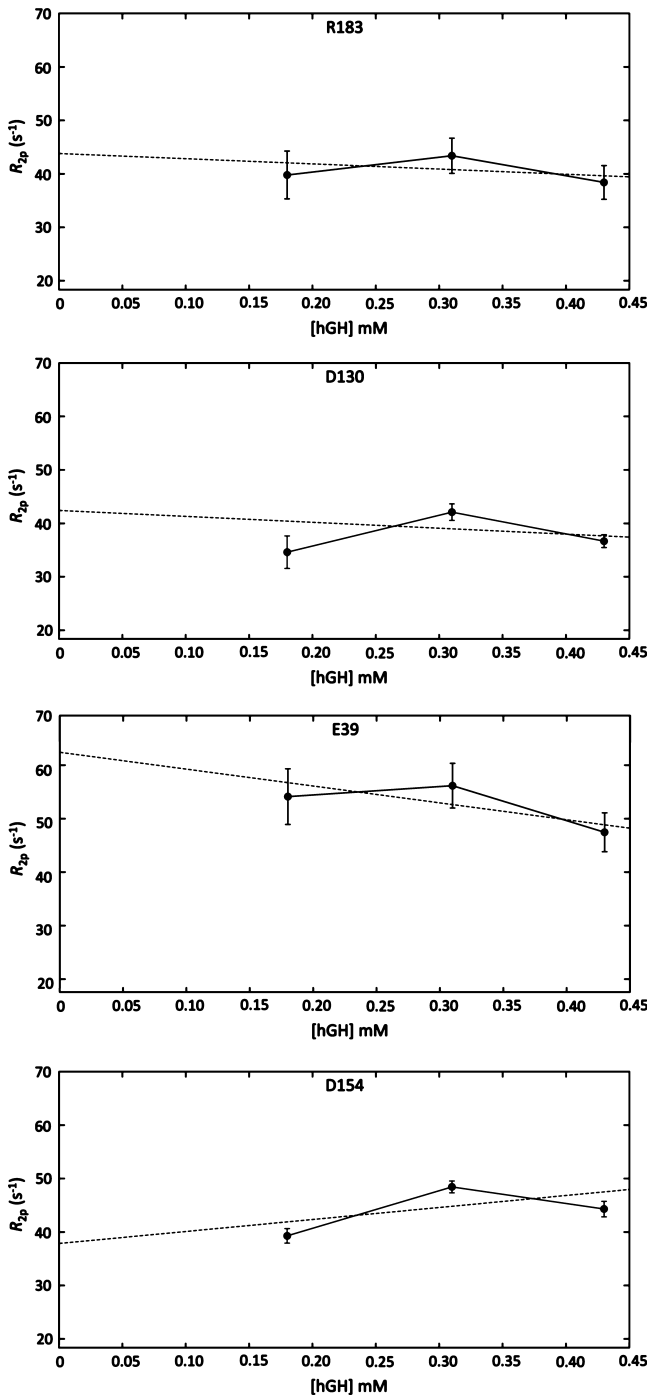


Figure 5. Examples of R_{2p} rates that decrease between 0.310 mM and 0.430 mM hGH. The four residues are located in the two interaction surfaces, patch 1 (R183, D130) and patch 2 (E39, D154), indicated in Figure 6, and may interact to form dimers (see text). Straight solid lines are drawn between the individual data points. The dashed lines are least-squares fit of the experimental R_{2p} rates.

rates in the hGH concentration range from 0.310 to 0.420 mM, may have a similar function.

The second patch with decreasing R_{2p} rates is located at the top of the molecule (patch 2, Figure 6B). It comprises the residues E39 and D154 with their negatively charged side chains protruding from the surface, the polar residue N99, and the three hydrophobic residues I36, A155, and L156. This negatively charged patch could interact with the positively

charged patch around R183 in patch 1, forming an asymmetric dimer. This dimer could aggregate further by binding another hGH molecule to each one of the two free ends and eventually form insoluble but reversible self-associates, as found experimentally at hGH concentrations slightly larger than those used here.⁸ The adjacent residues E88, Q91, F92, R94, A105, and S108 also have decreasing R_{2p} rates, which show that they may belong to the same interaction surface. The third patch with decreasing R_{2p} rates, which may form a binding interface, is located on the convex front of the molecule (patch 3, Figure 6C) and includes the residues G136, K140, Q141, T142, S144, K145, F146, D147, and T148 all in the major loop, 128–148, and E88 in helix 2 (72–92). Also, the adjacent residues S57, I58, T60, and S62 that are part of the 45–63 loop have decreasing R_{2p} rates, indicating participation in hGH-hGH associations.

The decreasing rates of H18 and D171 (Figure 6B) are interesting since the two residues form the end of the interhelical salt bridge network, H18-E174-H21-D171, that stabilizes the hGH molecule.^{48,49} Participation of these two residues in intermolecular interactions may weaken the salt bridges, destabilize the molecule, and expose hydrophobic residues. This may eventually lead to the formation of stronger intermolecular bonds with the interaction partners. In this context it is noteworthy that the breakage of the salt bridge network is a necessary prerequisite for the binding of hGH to its receptor.⁴⁴ Therefore, the ability of H18 and D171 to participate in intermolecular interactions, as found here, may be essential for the hGH–receptor interaction.

Concluding Remarks. It is found that the general Hwang-Freed model for spin relaxation by translational diffusion describes the PRE of amide protons in a protein caused by a paramagnetic cosolute only when crowding effects are taken into account. In that case, detailed information about ultraweak protein–protein interactions can be obtained directly from the PREs using the experimentally simple approach presented here, that is, an increasing protein concentration in combination with a constant concentration of the paramagnetic cosolute. Thus, the PREs of the residues that are affected only by transient, nonspecific protein–protein interactions increase linearly with the protein concentration, while the PREs of residues that are involved in more stable and specific protein–protein associations decrease at the higher concentrations because of specific protein–protein associations. This allows the specific interaction sites of the ultraweak protein–protein associations to be identified. However, the results reveal that ultraweak protein–protein aggregations, at least in the case of the hGH self-association, are not well-defined aggregations controlled by a few specific interactions. Rather, they depend on several weak interaction sites that cover a large part of the protein surface. In general the experimental approach described here may potentially be useful for characterizing the early stages of protein–protein interactions including self-associations. Finally, the differences in the local crowding effects may have important consequences for the use of solvent PREs in structure calculation protocols of protein–protein complexes.

MATERIALS AND METHODS

Preparation and Purification of hGH. Human growth hormone was expressed recombinantly in the BL21(DE3) strain of *Escherichia coli* and purified from inclusion bodies as previously described for human prolactin.⁵⁰ Uniform deuteration and ¹³C and ¹⁵N protein-labeling was achieved by growth of the recombinant bacteria in

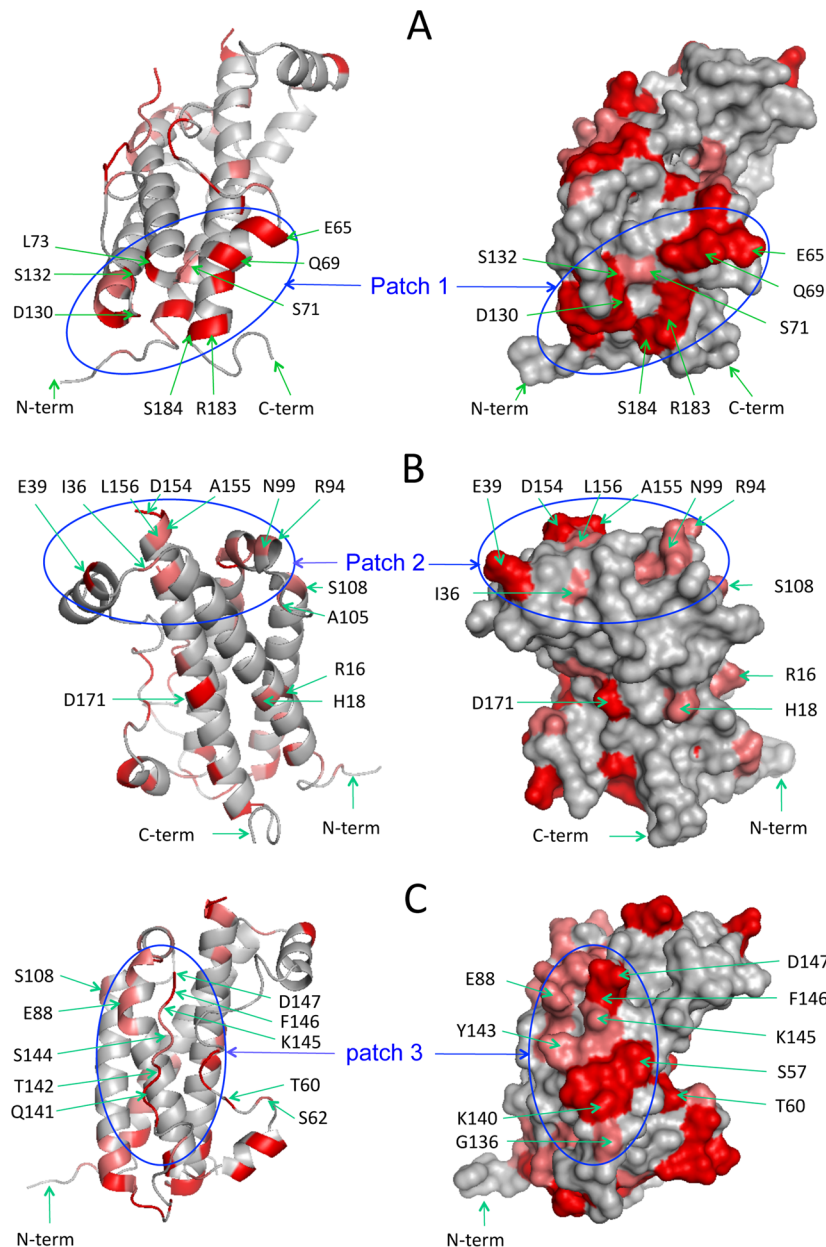


Figure 6. Residues with R_{2p} rates that decrease in the 0.310–0.430 mM hGH concentration range mapped onto the hGH structure (pdb: 3HHR); left column, ribbon models; right column, surface representations; red color, residues with $\Delta/\sigma_\Delta > 3$; salmon color, residues with $\Delta/\sigma_\Delta > 2$. The residues are located on or near to the surface and are grouped in patches indicating the interaction surfaces of the specific complexes. A, patch 1 at the bottom of the molecule; B, patch 2 at the top of the molecule; C, patch 3 on the convex front of the molecule including residues from the two major loops.

isotopically enriched M9 minimal media, prepared using 99.8% deuterated water with 1 g of $^{15}\text{N}-\text{NH}_4\text{Cl}$ and 3 g of U- $^{13}\text{C}_6$ -glucose (Cambridge Isotope Laboratories, Inc., Andover, MA) added per liter. Bacterial growth was initiated in a 50 mL starter culture of Luria broth (LB), with appropriately added antibiotics, until an OD_{600} reached approximately 0.6, followed by sequential inoculation and growth of the bacteria to the same cell density in 3:1 and 1:1 mixtures of the LB and labeled M9 minimal media, respectively, in order to accommodate the bacteria to progressive deuteration. Lastly, 0.5 mL aliquots of the final starter culture were used to inoculate eight 500 mL volumes of labeled M9 minimal media, followed by induction of protein expression and isolation of purified, refolded hGH using our standard protocol. The final yield was 80 mg of purified ^2H , ^{13}C , and ^{15}N -enriched hGH from a total of 4 L of bacterial culture.

Protein Samples. $[^2\text{H}, ^{15}\text{N}, ^{13}\text{C}]$ labeled hGH was dissolved in 25 mM phosphate buffer with 25 mM NaCl and azide and protease

inhibitors added. The spectra used for the chemical shift assignments were obtained from a 0.175 mM sample of the $[^2\text{H}, ^{15}\text{N}, ^{13}\text{C}]$ labeled hGH, pH 7 (meter reading) containing 1% D_2O (^{15}N HSQC, HNCO, HNCACO, HNCA, HNCACB, and NOESY TROSY experiments), or from a 1.0 mM sample of $[^{15}\text{N}, ^{13}\text{C}]$ -labeled hGH, pH 7 (meter reading) with 10% D_2O (^{15}N HSQC, HNCA, HNCO, HNCACB, and CBCA(CO)NH experiments). The assigned chemical shift data are deposited in the BMRB data bank, accession number 25029. For the paramagnetic relaxation enhancement experiments, the uniformly $[^2\text{H}, ^{15}\text{N}, ^{13}\text{C}]$ -labeled hGH samples were adjusted to a final hGH concentration of 0.180, 0.310, or 0.430 mM using Amicon Ultra Millipore with a pore size corresponding to 5000 Da. The protein concentration was determined by the absorption at 280 nm with a NanoDrop ND-1000 spectrophotometer. Subsequently, sodium azide and protease inhibitors (leupeptin, PMSF and pepstatin A) were added to a final concentration of 0.01%, 80 μM , 0.5 mM, and 0.8 $\mu\text{g}/\text{mL}$.

mL, respectively. All samples were adjusted to pH 7 (meter reading) with either HCl or NaOH, and gadodiamide (GE Healthcare) was added to a concentration of 4 mM and D₂O to a concentration of 7%. Two samples (0.126 mM and 0.460 mM hGH) were prepared without gadodiamide. All NMR samples were degassed and sealed under nitrogen. Attempts to increase the hGH concentration above ~0.55 mM eventually led to aggregation in the samples. Finally, the relative hGH concentrations of the three paramagnetic samples were confirmed by the ratios of the average intensity (volume) of 10 isolated signals in the HSQC spectra. The ratio of the intensities was 1.64 for the 0.310 mM and 0.180 mM samples, and 2.34 for the 0.430 mM and 0.180 mM samples, in good agreement with the concentration ratios 1.74 and 2.39, respectively.

NMR Experiments. NMR spectra were recorded at 298 K on a Bruker Avance 800 MHz spectrometer operating at a magnetic field strength of 18.7 T and equipped with a TCI cryoprobe. In all experiments the ¹H carrier was placed on the residual HDO resonance at 4.774 ppm at 298 K. A series of TROSY 2D and 3D heteronuclear NMR experiments was recorded to improve the assignment of hGH. Sensitivity enhanced ¹⁵N-¹H HSQC spectra were recorded as data sets with 1024 ¹H and 64 ¹⁵N complex data points and acquisition times of 80 ms (¹H) and 40 ms (¹⁵N), while HNCO spectra were recorded as data sets of 1024 ¹H × 32 ¹⁵N × 50 ¹³C complex data points with acquisition times of 71 ms (¹H), 20 ms (¹⁵N), and 15.5 ms (¹³C). Similarly, HN(CA)CO spectra were recorded as data sets of 1024 ¹H × 32 ¹⁵N × 50 ¹³C with acquisition times of 91 ms (¹H), 20 ms (¹⁵N), and 15.5 ms (¹³C), HNCA spectra as data sets of 1024 ¹H × 32 ¹⁵N × 64 ¹³C complex data points with acquisition times of 80 ms (¹H), 20 ms (¹⁵N), and 9.5 ms (¹³C), HN(CO)CA spectra as data sets of 1024 ¹H × 20 ¹⁵N × 32 ¹³C with acquisition times of 91 ms (¹H), 20 ms (¹⁵N), and 5 ms (¹³C), and HNCACB and CBCA(CO)NH spectra as data sets of 1024 ¹H × 32 ¹⁵N × 64 ¹³C complex points with acquisition times of 91 ms (¹H), 20 ms (¹⁵N), and 4.3 ms (¹³C). Nitrogen-15 edited NOESY spectra were obtained for the largely helical hGH to obtain and validate sequential ¹H-¹⁵N-¹H-¹⁵N assignments. The NOESY spectra were obtained with a mixing time of 120 ms as data sets of 1024 ¹H × 20 ¹⁵N × 64 ¹H data points with acquisition times of 91 ms (¹H), 13 ms (¹⁵N), and 7 ms (¹H).

¹H R₂ relaxation data were recorded as described by Donaldson et al.⁵¹ in experiments that sampled 1024 ¹H × 74 ¹⁵N complex points for 91 ms (¹H) and 41 ms (¹⁵N). Selective excitation of ¹H-¹⁵N resonances was performed with a 2.50 ms REBURP pulse centered at 8.25 ppm. Nine relaxation delays in the range between 6.5 and 60 ms (6.5, 10, 12, 15, 20, 25, 30, 40, and 60 ms) were used in order to sample the ¹H-¹⁵N decay in the presence of 4 mM gadodiamide, while nine relaxation delays in the range between 6.5 and 80 ms (6.5, 10, 15, 20, 25, 30, 40, 60, and 80 ms) were used for samples without gadodiamide.

Determination of the Paramagnetic Relaxation Enhancement. The relaxation rate was determined using the signal peak heights, and all the signals of a given residue in a relaxation experiment were analyzed simultaneously by a least-squares analysis. The R_{2p} rates were derived as

$$R_{2p} = R_{2exp} - R_{2d} \quad (7)$$

where R_{2exp} is the experimental relaxation rate obtained from the hGH samples containing gadodiamide, and R_{2d} is the corresponding diamagnetic relaxation rate. The estimated standard deviation of R_{2p} was calculated as $\sigma_{R_{2p}} = [(\sigma_{R_{2exp}})^2 + (\sigma_{R_{2d}})^2]^{1/2}$, where $\sigma_{R_{2exp}}$ and $\sigma_{R_{2d}}$ are the experimental errors (one standard deviation) of R_{2exp} and R_{2d}, respectively.

Estimation of the Deviation from Linear Concentration Dependence. The nonlinear concentration dependence of the three R_{2p} rates was estimated as the deviation, Δ, given by

$$\Delta = R_{2p}(c_2) - R_{2p}(\text{av}) \quad (8)$$

where

$$R_{2p}(\text{av}) = \frac{R_{2p}(c_3) - R_{2p}(c_1)}{c_3 - c_1} (c_2 - c_1) + R_{2p}(c_1) \quad (9)$$

and c₁, c₂, and c₃ are the three hGH concentrations. The uncertainty of Δ is given by

$$\sigma_\Delta = \sqrt{\sigma_{R_{2p}(\text{obs})}^2 + \sigma_{R_{2p}(\text{av})}^2} \quad (10)$$

where $\sigma_{R_{2p}(\text{av})}$ is given by

$$\sigma_{R_{2p}(\text{av})} = \sqrt{\sigma_{R_{2p}(c_3)}^2 \left(\frac{c_2 - c_1}{c_3 - c_1} \right)^2 + \sigma_{R_{2p}(c_1)}^2 \left(\frac{c_3 - c_2}{c_3 - c_1} \right)^2} \quad (11)$$

ASSOCIATED CONTENT

Supporting Information

Tables with assigned chemical shifts (S1), the R_{2exp} rates (S2), the R_{2d} rates (S3), the R_{2p} rates (S4), the R_{2p}(0) rates and the dependence of the R_{2p} rates on the hGH concentration (S5), the nonlinear concentration dependence of R_{2p} (S6), and the distances of closest approach, d (S7). The chemical shifts at pH 7.0 were deposited in the BioMagResBank (<http://www.bmrb.wisc.edu>) BMRB accession number 25029. This material is available free of charge via the Internet at <http://pubs.acs.org>.

AUTHOR INFORMATION

Corresponding Author

*E-mail: led@chem.ku.dk.

Present Address

¹Department of Drug Design and Pharmacology, University of Copenhagen, Universitetsparken 2, DK-2100 Copenhagen, Denmark.

Notes

The authors declare no competing financial interest.

ACKNOWLEDGMENTS

We thank M. A. S. Hass, S. M. Kristensen, D. F. Hansen, and J. Ø. Duus for helpful discussions during the initial stage of the study, D. Moskau, D. Boelskifte and B. Petersen for technical assistance, and the reviewers for useful suggestions. The 800 MHz spectra were acquired at the Danish Instrument Center for NMR Spectroscopy of Biological Macromolecules, which is supported by the Danish Agency for Science, Technology and Innovation (grant 276-06-0528) and Carlsberg Research Center. The gadodiamide was a gift from GE Healthcare, Denmark. Financial support was from the Danish Agency for Science, Technology and Innovation, grants 272-07-0466 and 645-06-0316 (JJL), The Lundbeck Foundation grant R58-A5181 (JJL), and the U.S. National Institutes of Health grant R01CA108992 (MEH).

REFERENCES

- Hansen, D. F.; Hass, M. A. S.; Christensen, H. M.; Ulstrup, J.; Led, J. *J. Am. Chem. Soc.* **2003**, *125*, 6858–6859.
- Volkov, A. N.; Worrall, J. A. R.; Holtzmann, E.; Ubbink, M. *Proc. Natl. Acad. Sci. U.S.A.* **2006**, *103*, 18945–18950.
- Bashir, Q.; Scanu, S.; Ubbink, M. *FEBS J.* **2011**, *278*, 1391–1400.
- Tang, C.; Iwahara, J.; Clore, G. M. *Nature* **2006**, *444*, 383–386.
- Fawzi, N. L.; Doucette, M.; Suh, J.-Y.; Clore, G. M. *Proc. Natl. Acad. Sci. U.S.A.* **2010**, *107*, 1379–1384.
- Kristensen, S. M.; Jørgensen, A. M. M.; Led, J. J.; Balschmidt, P.; Hansen, F. B. *J. Mol. Biol.* **1991**, *218*, 221–231.
- Chang, X.; Keller, D.; O'Donoghue, S. I.; Led, J. J. *FEBS Lett.* **2002**, *515*, 165–170.

- (8) Jensen, M. R.; Kristensen, S. M.; Keeler, C.; Christensen, H. E. M.; Hodsdon, M. E.; Led, J. J. *Proteins* **2008**, *73*, 161–172.
- (9) Tang, C.; Ghirlando, R.; Clore, G. M. *J. Am. Chem. Soc.* **2008**, *130*, 4048–4056.
- (10) Iwahara, J.; Clore, G. M. *Nature* **2006**, *440*, 1227–1230.
- (11) Suh, J.-Y.; Tang, C.; Clore, G. M. *J. Am. Chem. Soc.* **2007**, *129*, 12954–12955.
- (12) Hulsken, R.; Baranova, M. V.; George, G. S.; Bullerjahn, S.; Ubbink, M. *J. Am. Chem. Soc.* **2008**, *130*, 1985–1991.
- (13) Xu, X.; Reinle, W. G.; Hannemann, F.; Konarev, P. V.; Svergun, D. I.; Bernhardt, R.; Ubbink, M. *J. Am. Chem. Soc.* **2008**, *130*, 6395–6403.
- (14) Volkov, A. N.; Bashir, Q.; Worrall, J. A. R.; Ubbink, M. *J. Mol. Biol.* **2009**, *385*, 1003–1013.
- (15) Bashir, Q.; Volkov, A. N.; Ullmann, G. M.; Ubbink, M. *J. Am. Chem. Soc.* **2010**, *132*, 241–247.
- (16) Madl, T.; Bermel, W.; Zanger, K. *Angew. Chem., Int. Ed.* **2009**, *48*, 8259–8262.
- (17) Madl, T.; Güttler, T.; Görlich, D.; Sattler, M. *Angew. Chem., Int. Ed.* **2011**, *50*, 3993–3997.
- (18) Blundell, T. L.; Fernandez-Recio, J. *Nature* **2006**, *444*, 279–280.
- (19) Ubbink, M. *FEBS Lett.* **2009**, *583*, 1060–1066.
- (20) Schreiber, G.; Haran, G.; Zhou, H.-X. *Chem. Rev.* **2009**, *109*, 839–860.
- (21) Pintacuda, G.; Otting, G. *J. Am. Chem. Soc.* **2002**, *124*, 372–373.
- (22) Hwang, L.-P.; Freed, J. H. *J. Chem. Phys.* **1975**, *63*, 4017–4025.
- (23) Freed, J. H. *J. Chem. Phys.* **1978**, *68*, 4034–4037.
- (24) Luz, Z.; Meiboom, S. *J. Chem. Phys.* **1964**, *40*, 2686–2692.
- (25) Solomon, I. *Phys. Rev.* **1955**, *99*, 559–565.
- (26) Bertini, I.; Luchinat, C.; Parigi, G. *Solution NMR of Paramagnetic Molecules. Applications to Metallobiomolecules and Models*; Elsevier: Amsterdam, 2001.
- (27) Lester, C. C.; Bryant, R. G. *J. Phys. Chem.* **1990**, *94*, 2843–2847.
- (28) Kao, H. P.; Abney, J. R.; Verkman, A. S. *J. Cell Biol.* **1993**, *120*, 175–184.
- (29) Zorrilla, S.; Hink, M. A.; Visser, A. J.; Lillo, M. P. *Biophys. Chem.* **2007**, *125*, 298–305.
- (30) Dix, J. A.; Verkman, A. *Annu. Rev. Biophys.* **2008**, *37*, 247–263.
- (31) Kasimova, M. R.; Kristensen, S. M.; Howe, P. W. A.; Christensen, T.; Matthiesen, F.; Petersen, J.; Sørensen, H. H.; Led, J. J. *J. Mol. Biol.* **2002**, *318*, 679–695.
- (32) Dauty, E.; Verkman, A. S. *J. Mol. Recognit.* **2004**, *17*, 441–447.
- (33) Wang, Y.; Spiller, M.; Caravan, P. *Magn. Reson. Med.* **2010**, *63*, 609–616.
- (34) Powell, D. H.; Dhubghaill, O. M. N.; Pubanz, D.; Helm, L.; Lebedev, Y. S.; Schlaepfer, W.; Merbach, A. E. *J. Am. Chem. Soc.* **1996**, *118*, 9333–9346.
- (35) Elst, L. V.; Sessoye, A.; Laurent, S.; Muller, R. *Helv. Chim. Acta* **2005**, *88*, 574–587.
- (36) Kestin, J.; Sokolov, M.; Wakeham, W. A. *J. Phys. Chem. Ref. Data* **1978**, *7*, 941–948.
- (37) Einstein, A. *Ann. Phys.* **1905**, *17*, 549–560.
- (38) Koedermann, T.; Ludwig, R.; Paschek, D. *ChemPhysChem* **2008**, *9*, 1851–1858.
- (39) Fernandez-Fuentes, N.; Zhai, J.; Fiser, A. *Nucleic Acids Res.* **2006**, *34*, W173–W176.
- (40) Sanner, M. F.; Olson, A. J.; Spehner, J. C. *Biopolymers* **1996**, *38*, 305–320.
- (41) Cock, P. J. A.; Antao, T.; Chang, J. T.; Chapman, B. A.; Cox, C. J.; et al. *Bioinformatics* **2009**, *25*, 1422–1423.
- (42) Schreiber, G.; Fersht, A. R. *Nat. Struct. Biol.* **1996**, *3*, 427–431.
- (43) Zhang, X.; Lam, V. Q.; Mou, Y.; Kimura, T.; Chung, J.; Chandrasekar, S.; Winkler, J. R.; Mayo, S. L.; Shan, S. O. *Proc. Natl. Acad. Sci. U.S.A.* **2011**, *108*, 6450–6455.
- (44) de Vos, A. M.; Ultsch, M.; Kossiakoff, A. A. *Science* **1992**, *255*, 306–312.
- (45) Argos, P. *Protein Eng.* **1993**, *2*, 101–113.
- (46) Clackson, T.; Wells, J. A. *Science* **1995**, *267*, 383–386.
- (47) Bogan, A. A.; Thorn, K. S. *J. Mol. Biol.* **1998**, *280*, 1–9.
- (48) Abildgaard, F.; Jørgensen, A. M. M.; Led, J. J.; Christensen, T.; Jensen, E. B.; Junker, F.; Dalbøge, H. *Biochemistry* **1992**, *31*, 8587–8596.
- (49) Vinther, J. M.; Kristensen, S. M.; Led, J. J. *J. Am. Chem. Soc.* **2011**, *133*, 271–278.
- (50) Keeler, C.; Dannies, P. S.; Hodsdon, M. E. *J. Mol. Biol.* **2003**, *328*, 1105–1121.
- (51) Donaldson, L. W.; Skrynnikov, N. R.; Choy, W.-Y.; Muhandiram, D. R.; Sarkar, B.; Forman-Kay, J. D.; Kay, L. E. *J. Am. Chem. Soc.* **2001**, *123*, 9843–9847.